Spectral CT in Oncology

Onkologische Bildgebung mittels Spektral-CT

Authors
Julia Sauerbeck, Gerhard Adam, Mathias Meyer

Affiliation
Department of Diagnostic and Interventional Radiology and Nuclear Medicine, University Medical Center Hamburg-Eppendorf, Hamburg, Germany, Hamburg, Germany

Key words
therapy planning, oncology imaging, lesion detection, review, CT, spectral CT

received 26.10.2021
accepted 03.07.2022
published online 27.09.2022

Bibliography
Fortschr Röntgenstr 2023; 195: 21–29
DOI 10.1055/a-1902-9949
ISSN 1438-9029

Georg Thieme Verlag KG, Rüdigerstraße 14, 70469 Stuttgart, Germany

Correspondence
Dr. Mathias Meyer
Department of Diagnostic and Interventional Radiology and Nuclear Medicine, University Medical Center Hamburg-Eppendorf, Hamburg, Germany, Martinistraße 52, 20246 Hamburg, Germany
Tel.: +49/40/7 41 05 40 10
mat.meyer@uke.de

ABSTRACT

Background Spectral CT is gaining increasing clinical importance with multiple potential applications, including oncological imaging. Spectral CT-specific image data offers multiple advantages over conventional CT image data through various post-processing algorithms, which will be highlighted in the following review.

Methodology The purpose of this review article is to provide an overview of potential useful oncologic applications of spectral CT and to highlight specific spectral CT pitfalls. The technical background, clinical advantages of primary and follow-up spectral CT exams in oncology, and the application of appropriate spectral tools will be highlighted.

Results/Conclusions Spectral CT imaging offers multiple advantages over conventional CT imaging, particularly in the field of oncology. The combination of virtual native and low monoenergetic images leads to improved detection and characterization of oncologic lesions. Iodine-map images may provide a potential imaging biomarker for assessing treatment response.

Key Points:

- The most important spectral CT reconstructions for oncology imaging are virtual unenhanced, iodine map, and virtual monochromatic reconstructions.
- The combination of virtual unenhanced and low monoenergetic reconstructions leads to better detection and characterization of the vascularization of solid tumors.
- Iodine maps can be a surrogate parameter for tumor perfusion and potentially used as a therapy monitoring parameter.
- For radiotherapy planning, the relative electron density and the effective atomic number of a tissue can be calculated.

Citation Format

- Sauerbeck J, Adam G, Meyer M. Onkologische Bildgebung mittels Spektral-CT. Fortschr Röntgenstr 2023; 195: 21–29

ZUSAMMENFASSUNG

Hintergrund Die Spektral-CT gewinnt mit vielfältigen Einsatzmöglichen zunehmend an klinischer Bedeutung, so auch im Rahmen der onkologischen Bildgebung. Die Spektral-CT-spezifischen Bilddaten bieten durch verschiedene Nachbearbeitungsalgorithmen vielfältige Vorteile gegenüber konventionellen CT-Bilddaten, was im folgenden Review genauer beleuchtet werden soll.

Methodik Der vorliegende Review-Artikel soll einen Überblick über die potenziell nützlichsten onkologischen Anwendungsgebiete der Spektral-CT geben und auf spezifische Spektral-CT-Fallsticke hinweisen. Hierbei werden sowohl technische Hintergründe als auch klinische Vorteil von onkologischen Primär- und Verlaufsuntersuchungen mittels Spektral-CT beleuchtet und die Anwendung entsprechender Spektral-Tools erläutert.

Ergebnisse/Schlussfolgerungen Die Spektral-CT-Bildgebung bietet vielfältige Vorteile gegenüber der konventionellen CT-Bildgebung, insbesondere auf dem Gebiet der Onkologie. Die Kombination von virtuell nativen und niedrigenergetischen Bildern führt zu einer verbesserten Detektion und Charakterisierung von Tumorläsionen. Jodkarten-Bilder bieten einen potenziellen Imaging-Biomarker zur Beurteilung des Therapieansprechens.

Introduction

Thanks to increasing availability, spectral CT systems are more frequently being used in daily clinical routine. Spectral CT, which allows specific material characterization, can be used for a number of different applications in oncological imaging [1]. In addition to improved detection and characterization of malignant lesions, spectral CT allows precise treatment planning and provides a novel imaging biomarker for tumor vitality [2–5]. This article discusses specific spectral CT systems and spectral reconstructions with a focus on oncological applications. In addition, spectral CT-specific pitfalls that need to be known in order to avoid interpretation errors are discussed.

Basics of spectral CT imaging

While conventional CT imaging is based on differences in physical density between two neighboring structures, spectral CT imaging is based on differences in the basic composition of structures [6]. By examining two different energy spectra, structures with a similar density but a different basic composition can be differentiated from one another based on differences in photon absorption. This material-specific imaging allows, for example, selective visualization and quantification of intravenously applied iodine. However, only materials with a strong photoelectric effect, e. g., calcium, iodine, barium, and xenon, can be differentiated from other body tissues like fat with a weak photoelectric effect. The two typically used energy spectra have a peak of 70–100 kilovolts (kVp) (low energy spectrum) and 140–150 kVp (high energy spectrum) [1].

All currently available clinical CT systems that offer spectral imaging can be classified into two groups: emission-based and detector-based systems [7]. Emission-based systems use X-ray beams with different energy spectra. This can be achieved either by using two independent X-ray tubes with one tube generating a low energy and the other having a high energy or by using a single X-ray tube that quickly switches between low and high energies. A further possibility for creating different energy spectra using only one X-ray source is to use a split beam with two different filters, e. g. of tin and gold, during a 360° rotation, thus allowing filtration into a low and a high energy spectrum [8]. Detector-based systems are based on the detector's ability to separate energies by separating the signals of the low-energy X-ray photons from the high-energy photons. This separation can be achieved using a dual-layer energy-integrating detector with different photon registration in every layer (e. g., using an yttrium-based scintillator) or a photon-counting detector. The most common and most widely available clinical spectral CT systems in Europe [2–4] are the dual-source CT system (e. g., SOMATOM Force or SOMATOM Definition Flash, Siemens Healthineers), which is an emission-based system with two independent X-ray tubes, the dual-layer CT system (e. g., IQon Spectral CT, Philips Healthcare), which is a detector-based system with a dual-layer detector, and the ultrafast switching CT system (e. g., Discovery HD, GE Healthcare), which is an emission-based system with a single fast-switching X-ray tube. The first clinical photon-counting detector CT system introduced last year (NAEOTOM Alpha; Siemens Healthineers), which allows improved spectral separation, is not discussed here due to the small number of clinical studies available.

Image reconstruction of spectral CT datasets

Selective quantification of elements such as iodine can be achieved by a two- or three-material decomposition algorithm in the projection domain (Ultrafast switching and dual-layer CT systems) or in the image domain (dual-source CT systems) [7]. The following section describes the most common spectral CT image reconstructions in oncological imaging.

Material density maps

Manufacturer-specific material decomposition algorithms can be used to create material density maps that selectively display or remove materials. The most clinically relevant application in oncology is the material density map that shows iodine or calcium and to a lesser degree also the relative electron density and the effective atomic number. These maps allow selective fading out of the soft-tissue background while highlighting specific materials, the relative electron density, and the effective atomic number. Among other things, these material density maps make it possible to characterize vascularized and non-vascularized lesions (in the case of iodine maps), an important criterion for the characterization of kidney or liver lesions [9].

On virtual non-contrast (VNC) CT images and virtual non-calcium (VNCa) CT images, certain materials like iodine and calcium are selectively suppressed [7]. VNC images with selective suppression of iodine are comparable to true unenhanced images, which are normally acquired prior to contrast administration in the case of certain clinical questions. In oncological imaging, these images are often needed for the characterization, for example, of incidental renal lesions during an initial staging examination [10, 11]. Other applications include the differentiation between therapy-induced tumor hemorrhages and calcifications [12]. Due to the possibility of eliminating a true non-contrast CT examination, the radiation dose can be reduced [13]. This is an important aspect of curative treatment approaches because the cumulative radiation dose of imaging follow-up examinations can be significant [14].

Selective imaging of bone marrow involvement using VNCa maps e. g., in patients with multiple myeloma, can facilitate the detection of focal lesions and the differentiation between osteoporotic changes and plasma cell infiltration [15, 16].

Virtual monochromatic images (VMI)

The term polychromatic X-ray beam relates to an X-ray beam with a full energy spectrum in which the kVp represents the upper limit of the energy spectrum. It should be noted that low-energy photons of this polychromatic X-ray beam are responsible for a disproportionately high proportion of background image noise and image artifacts (e. g. beam hardening artifacts). Spectral imaging can be used to create virtual monochromatic images (VMI) from material-specific images using a complex algorithm [7]. These are then comparable with image data that would be generated with a theoretical monochromatic beam. The X-ray energy is measured

▶ **Table 1** Image types and techniques of the 3 most common spectral CT systems and most important applications in oncology.

Technique/Reconstruction	Siemens Healthineers	Philips Healthcare	GE Healthcare
Name of viewer	**Syngo.via**	**Intellispace portal**	**Advantage workstation**
Image reconstruction domain	Image	Projection	Projection
No. of material decomposition techniques	3	2	2
Virtual monochromatic images	Virtual monoenergetic or mono-energetic plus	Monoenergetic (MonoE)	VMC
Kiloelectronvolt (keV)	40–190	40–200	40–140
Oncological applications	Lesion detection and demarcation from surrounding tissue, enhanced vascular contrast e. g., acute pulmonary artery embolism detection		
Material decomposition images Iodine maps	Liver virtual non-contrast (liver only); virtual non-contrast (all other organs)	Iodine no water, Iodine density	Iodine (water/fat)
Unit of measure	1 mg/mL	1 mg/mL	100 µg/cm^3
Oncological applications	Characterization of lesion vascularization, therapy monitoring including detection of tumor hemorrhages and calcifications		
Virtual non-contrast images	Liver virtual non-contrast (only for liver); virtual non-contrast (for all other organs)	Virtual unenhanced	Virtual unenhanced
Unit of measure	Hounsfield unit (HU)	HU	HU
Oncological applications	Characterization of lesion vascularization, therapy monitoring with detection of tumor hemorrhages and calcifications		
Virtual non-calcium image	Bone removal, bone marrow	Calcium suppressed	Iodine (calcium)
Unit of measure	Hounsfield unit (HU)	HU	HU
Oncological applications	Detection of bone marrow malignancies		

in kiloelectron volt (keV) instead of kVp and the VMI spectrum is 40–200 keV with manufacturer-specific differences (see ▶ **Table 1**). VMI image data reconstructed between 75–77 keV are comparable with image data from a polychromatic X-ray beam with 120 kVp. Low-energy VMI images (40–60 keV) result in higher iodine absorption due to the closeness to the k-edge of iodine (33 keV), leading to enhanced iodine contrast on the image [17]. This has a number of advantages for oncological imaging. Among other things, low-energy VMI images make it possible to detect lesions, e. g. hypervascularized liver metastases, with greater sensitivity [18]. In the case of high-energy VMC images (170–200 keV), artifacts caused by foreign materials, e. g., dental prostheses or prosthetic joints, can be reduced, resulting in better assessment of the size of lesions in the immediate vicinity of such foreign objects [19].

Oncological applications

Improved detection of oncological lesions

By using low-energy VMI images or iodine maps, hypervascularized as well as faint hypodense lesions can be better delimited from parenchymatous background tissue (▶ **Fig. 1**). VMI reconstructions between 50–55 keV provide the best contrast-to-noise ratio for the majority of parenchymatous organs. However, it should be noted that other keV reconstructions (e. g. 70 keV) are more suitable in highly vascularized tissue (e. g. renal parenchyma) [20–22]. A number of studies were able to show the advantage of these two spectral CT reconstructions for malignancies in the head-neck/neck region for primary and secondary hepatic masses and pancreatic malignancies in which the lesion-to-tissue contrast is intrinsically lower [23]. For example, in the case of hepatic steatosis, either medically (e. g. during chemotherapy) or metabolically induced, it is often challenging to detect faint hypovascularized lesions on conventional CT. By using low-energy VMI images or iodine maps, improved lesion-to-tissue contrast can be achieved because the lesion has a greater density while the fatty liver tissue appears hypodense. Thus, in particular, hepatocellular carcinomas, cholangiocellular carcinomas, and hepatic metastases can be better detected.

In patients with bone marrow involvement in a malignant disease, e. g., multiple myeloma, MRI has been the imaging method of choice. Using spectral VNCa image data, both focal bone marrow lesions (> 1 cm) and the pattern of involvement can be detected with a similar accuracy to that of MRI with equally precise detection of osteolytic bone lesions [15, 16]. This is an advantage compared to conventional CT in which trabecular bone structures currently cannot be sufficiently extracted making detection as well as the differentiation between plasma cell infiltration and osteoporotic bone demineralization difficult (▶ **Fig. 2**). However, it

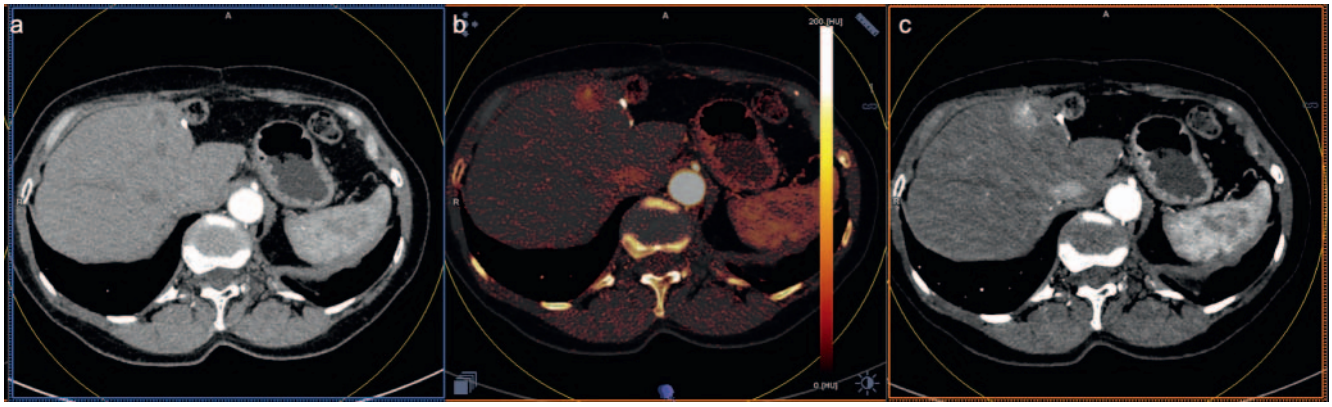

▶ **Fig. 1** 66-year-old female patient with metastatic clear cell renal cell carcinoma to the liver who had undergone previous atypical partial liver resection. At best, a faint hypervascularized lesion can be detected at the margins of the atypical liver resection in the 120 kVp equivalent images **a**. The iodine map images reconstructed from spectral CT **b** and virtual monoenergetic images at 50 keV **c** clearly show the hypervascularized portions of the lesion.

must be noted that the currently available clinical spectral CT systems allow the generation of VNCa image data only from non-contrast spectral CT examinations. Therefore, clinical application is currently limited. In the future, the use of the aforementioned clinical photon-counting detector CT systems could be expanded to include contrast-enhanced CT examinations [24].

Patients with a malignancy have an increased risk of pulmonary embolism [25]. Depending on the phase, pulmonary embolisms are sometimes overlooked in staging examinations, which are primarily performed in a portal venous phase [26]. Both low-energy VMI images and iodine maps provide better detection of pulmonary embolisms due to the improved thrombus-to-vessel contrast or the evaluation of a filling defect within the vessel (▶ **Fig. 3**) [27].

Characterization of oncological lesions

Detection of vascularization of solid masses is an important clinical objective of all imaging methods since it can help to characterize masses. In conventional staging CT examinations performed in a single phase, incidentally detected lesions, particularly adrenal and renal lesions often cannot be characterized in greater detail (Fig, 4, 5). As a result, it is recommended to perform supplementary imaging, follow-up examination, or biopsy. Spectral CT imaging can provide important additional information both in primary staging and in follow-up examinations with various image reconstructions and allow early characterization [2–5]. This can reduce the patient's emotional burden, accelerate the introduction of an appropriate treatment regimen, and reduce treatment costs.

VNC images or iodine maps reconstructed from a spectral CT dataset allow differentiation between a vascularized and non-vascularized lesion which is particularly helpful for the differentiation between a hemorrhagic/protein-rich cyst and a solid hepatic or renal mass [9, 28]. Based on the cutoff value of true non-contrast image data, a vascular lesion is defined as an increase in the density (measured in Hounsfield units (HU)) between the VNC and the contrast-enhanced image data of > 20 HU [29]. When using iodine maps, there are manufacturer-specific differences regarding the definition of a contrast-enhancing lesion with iodine concentration cutoff values ranging from 0.5 mg/mL to 2.0 mg/mL [30–32]. For the dual-source CT systems most commonly available in Germany, a cutoff value of 0.5 mg/mL has been established [4]. Iodine maps can also be helpful for the differentiation between thromboses without iodine uptake and a tumor thrombus with iodine uptake, e. g. in hepatocellular carcinoma or renal cell carcinoma with venous infiltration.

VNC images and specific material density maps can also provide additional information about the composition of a lesion, particularly about fatty, hemorrhagic, or faint calcified areas [1]. For example, this is helpful in the characterization of adrenal masses, in which fat-isodense lesion portions (density values in the VNC datasets < 10 HU) indicate an adenoma [33]. The differentiation, for example, between a postoperative hematoma and a new metastasis can be difficult in the case of conventional single-phase CT. However, VNC images or iodine maps can be used for precise characterization without supplementary imaging.

Treatment planning and treatment monitoring

Precise knowledge of tumor location, extent, and relationship to surrounding tissue and vascular structures is important for treatment planning. In particular, image-based therapeutic methods like radiofrequency ablation, stereotactic radiotherapy, and intraarterial therapies (e. g. selective internal radiotherapy or transarterial chemoembolization) require imaging that is as exact as possible in order to facilitate planning.

VMI images in the low-energy range and iodine maps with a higher lesion-to-noise ratio allow better differentiation of a tumor lesion from surrounding structures like vessels and adjacent organs and exact determination of the number and size of lesions. Particularly in liver or head/neck tumors, the determination of lesion margins compared to surrounding tissue can be difficult on conventional CT imaging [34–36]. VMI images in the high-energy range can greatly reduce metal artifacts thus allowing better delimitation of the area to be scanned, which can be advantageous, for example, in the case of head/neck tumors with artifacts from dental fillings [37].

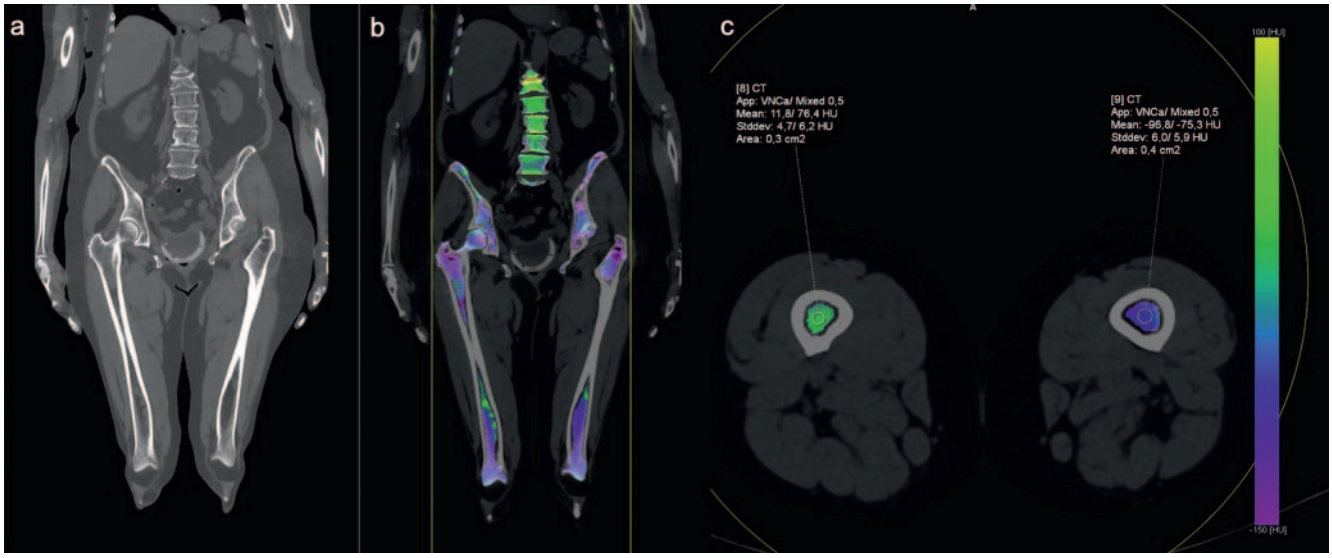

▶ **Fig. 2** 76-year-old patient with histologically confirmed multiple myeloma. **a** Conventional CT shows an inhomogeneous bone structure of the lumbar spine and femora, but it is not possible to clearly differentiate between osteoporotic changes and multiple myeloma involvement. In the virtual non-calcium images calculated from spectral CT in coronary **b** and axial **c** reconstructions, bone marrow edema of the lumbar spine and distal metaphyseal femora with density values of 12 HU compared to healthy fatty bone marrow of –97 HU is shown as an indication of plasma cell infiltration related to multiple myeloma.

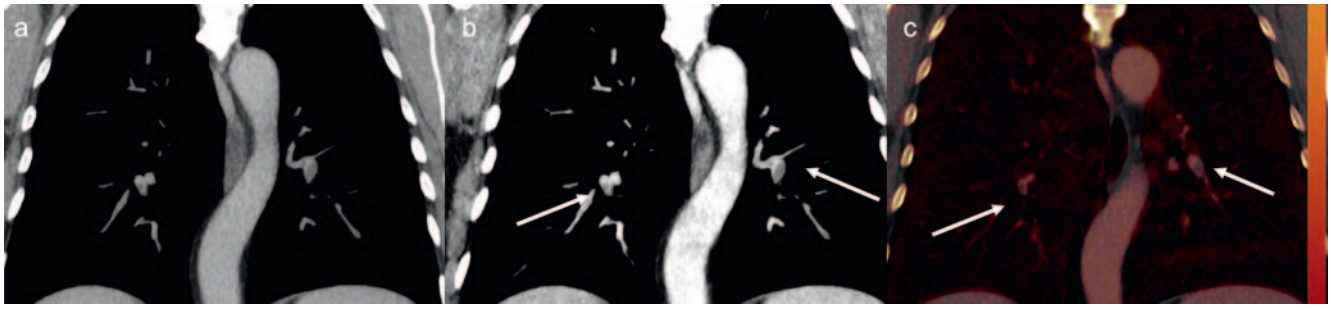

▶ **Fig. 3** 75-year-old female patient with metastatic malignant melanoma undergoing immunotherapy. In the 120 kVp-equivalent images **a**, a faint filling defect of the lower lobe arteries can be seen. Virtual monoenergetic images reconstructed from spectral CT at 45 keV **b** and iodine map images **c** show a clear filling defect suggestive of segmental pulmonary embolism.

Spectral CT imaging makes it possible to estimate the relative electrode density (ρe) and the effective atomic number (Z_{eff}). Determination of these tissue parameters is of particular interest for dose calculation in radiation therapy treatment planning. They can be used either directly (e. g. the relative electron density) or as a substitute for other parameters (e. g., the effective atomic number as replacement for the average excitation energy) to calculate the stopping power ratio [38].

The objective evaluation of treatment response to systemic or local treatment is important to monitor the effect of oncological treatments so that treatment changes can be implemented as early as possible. The established and currently used imaging criteria for evaluating response, e. g. the "Response Evaluation Criteria in Solid Tumors" (RECIST1.1) and the modified versions (iRECIST and irRECIST), are based on serial measurement of tumor size. However, purely size-based response criteria overestimate and underestimate the treatment success of modern therapies that are not necessarily cytotoxic but rather cytostatic and thus do not necessarily result in a change in size. The treatment effect can be better quantified by biomarkers that characterize tumor vitality (e. g. metabolic or diffusion-weighted imaging) [39]. Spectral CT imaging provides advantages here compared to conventional CT since it allows differentiation between iodine uptake in vital tumor tissue after i. v. contrast injection and, for example, treatment-induced tumor hemorrhage (▶ **Fig. 6**) [40]. Additional advantages include the elimination of errors that can occur in connection with a spatial misregistration between non-contrast and contrast-enhanced datasets (e. g., due to a different breathing positions between the examinations). In particular, vitality quantification based on iodine maps is a promising approach that could have an advantage over the above-mentioned purely size-based response criteria both in systemic therapies (e. g. gastrointestinal stromal tumor under systemic tyrosine kinase inhibitor therapy) [41] and in locally ablative methods (e. g., evaluation of the short-term and long-term treatment success after hepatic and renal radiofrequency/microwave ablation) [42].

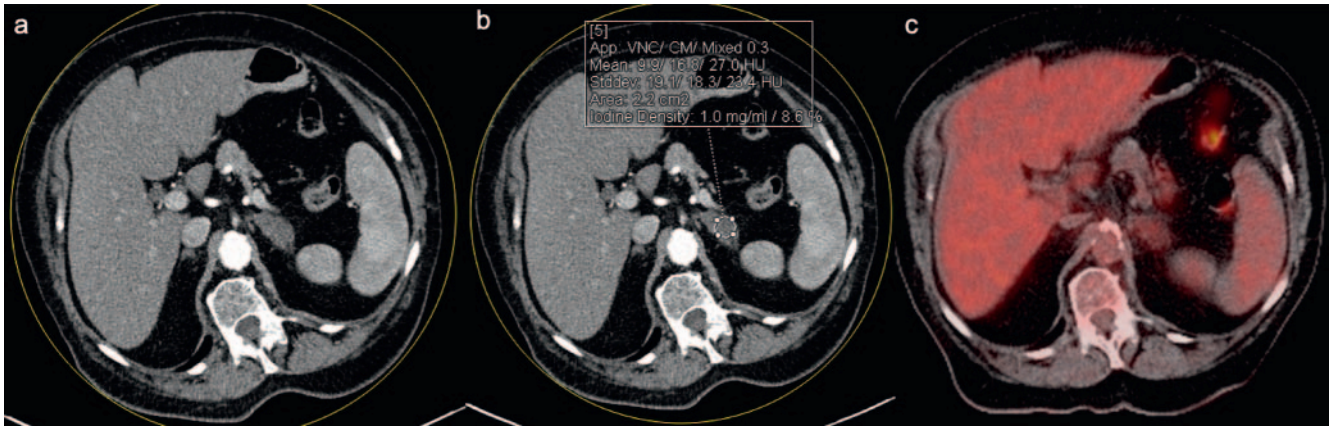

▶ **Fig. 4** 53-year-old patient with a T1c bronchial carcinoma and incidentaloma of the left adrenal gland. In the 120 kVp equivalent images **a**, the mass has density values averaging 27 HU. The VNC and iodine map images calculated from spectral CT **b** give density values of < 10 HU (VNC) and an iodine uptake of 1 mg /mL. Thus, the mass represents an adrenal adenoma, which is confirmed in the subsequent guideline-oriented FDG-PET-CT examination **c**, in which the adrenal mass shows no increased metabolic activity.

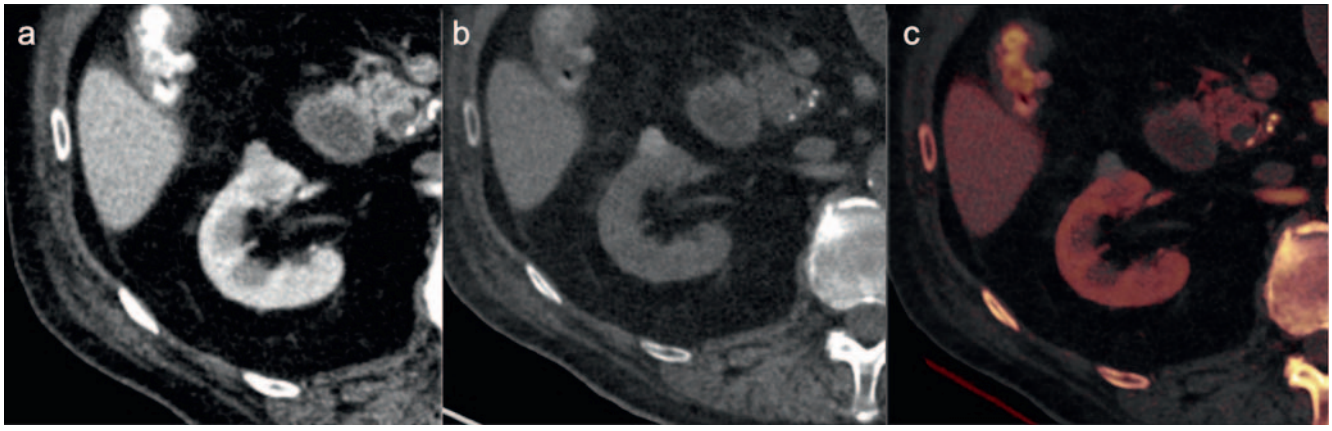

▶ **Fig. 5** 68-year-old patient with detection of an exophytic hyperdense lesion ventrally in the middle bulb of the right kidney. The mass has density values of 99 HU on the 120 kVp equivalent images **a**. Given this image, it is not possible to differentiate between a hemorrhagic renal cyst and renal cell carcinoma with certainty. The VNC **b** and iodine map images **c** calculated from spectral CT already show a density enhancement (91 HU) in the VNC images and no relevant iodine uptake (0.3 mg/mL) in the iodine map images. Thus, the lesion corresponds to a hemorrhagic renal cyst (Bosniak II) and was constant in size over 3 years.

Artifacts and pitfalls

Based on the special reconstructions algorithms, there are specific artifacts and pitfalls with regard to spectral CT. As in the case of conventional polychromatic image data, the density values of VMI image data depends on the energy. Therefore, for example, the liver parenchyma can be 110H HU at 50 keV, 80 HU at 70 keV, and 65 HU at 140 keV [43]. Thus, the above-mentioned determination of the cutoff value for contrast enhancement can only be applied to VMI images that are equivalent to a polychromatic image dataset at 120 kVp (75–77 keV).

Numerous studies were able to demonstrate an excellent correlation between the density values of VNC images and true non-contrast image data with density differences < 5 HU [11, 44–52]. However, it should be noted that the density values for VNC images are subject to various influencing factors, e. g. patient habitus or the contrast phase, with some differences between VNC and true non-contrast image data being significant, which can result in an incorrect classification of lesions [11, 52]. A common cause of these discrepancies is incomplete subtraction of iodine from VNC images, which can be observed, in particular, in image areas with a very high iodine concentration. For example, contrast pooling in the pelvicalyceal system can result in incomplete subtraction, resulting in incorrectly high density values in the VNC images, leading to a risk of misinterpretation of blood clots or calcifications within the pelvicalyceal system. It should be noted that the application of iodine-containing materials, e. g., lipiodol in transarterial chemoembolization, results in a subtraction from the VNC images, thus complicating post-interventional characterization of remaining vital portions.

Moreover, calcium is selectively characterized using a cutoff value on iodine maps as well as VNC images. This results in small (< 2 mm) or faint calcifications (< 380 HU) being incorrectly extracted from the VNC image [53, 54]. This effect is enhanced

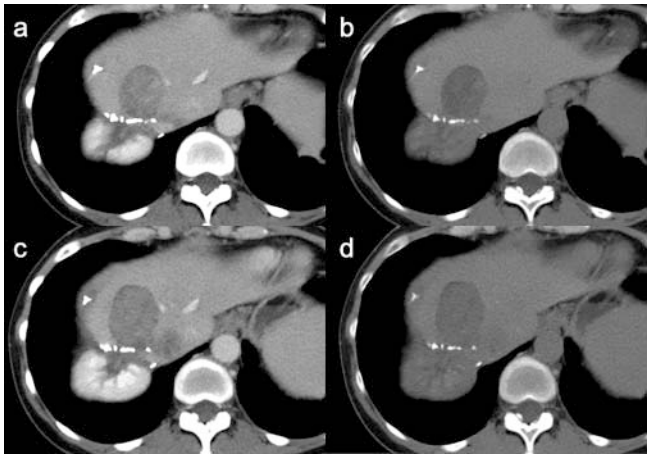

▶ **Fig. 6** 51-year-old female patient with a metastatic gastrointestinal stromal tumor to the liver on sunitinib therapy on baseline CT (a–b) and follow-up CT after 3 months (c–d). Baseline spectral CT scan shows a vital tumor fraction with a difference between virtual unenhanced images **a** and 120 kVp equivalent images **b** of 47 HU (25 HU to 73 HU). Follow-up spectral CT examination shows a size progression of the lesion with diffuse density-enhanced portions within the lesion. The differences between the virtual unenhanced images **c** and the 120 kVp equivalent images **d** is 6 HU (64 HU to 70 HU) and suggests a pseudoprogression with intra-tumoral hemorrhage under sunitinib therapy. This is confirmed in the follow-up examinations, where the lesion shows a stable size again without vital tumor portions.

particularly in the case of images with high background noise, for example, in obese patients. In these cases, a true non-contrast examination can sometimes be indicated.

Clinically accepted areas of application

In spite of the numerous potential applications of spectral CT mentioned above, only VMI and VNC image data has achieved clinical acceptance so far. For lesion detection and determination of the local size of hypervascularized lesions (e. g., hepatocellular carcinoma, clear cell renal cell carcinoma metastases, and neuroendocrine tumors) and head-neck tumors, VMI image data in the low-energy range (50–55 keV) should be used as the primary image data due to the improved lesion-to-tissue contrast and resulting increased diagnostic accuracy [21, 34].

VNC image data have become clinically established particularly in the evaluation of the macroscopic fat components of incidentalomas and renal masses due to their high diagnostic accuracy [11, 33, 34]. Precisely characterizing these lesions in single-phase CT examinations avoids additional radiation exposure with multiphase CT examinations, subsequent costs incurred by additional examinations, and patient uncertainty. In the case of explicit characterization of renal lesions or adrenal lesions, using VNC datasets and consequently dispensing with a true non-contrast examination reduces the radiation by one third (e. g. characterization of renal lesions: spectral nephrographic phase including VNC image data and washout phase instead of a non-contrast, nephrographic, and washout phase). In patients undergoing treatment with tyrosine kinase inhibitors (e. g., imatinib) or monoclonal antibodies (e. g., bevacizumab or nivolumab) with single-phase CT staging examinations, VNC image data should always also be considered to differentiate rare pseudoprogression caused by a tumor hemorrhage from true progression [4, 11].

Conclusion

There are a number of possible applications for spectral CT in oncological imaging. In particular, VMI image data in the low-energy range (e. g. 50–55 keV), iodine maps, and VNC images provide advantages regarding the detection of, e. g., hypervascularized tumors and the differentiation between vascularized and non-vascularized liver or kidney lesions. Iodine quantification with respect to a tumor provides a potential biomarker for the assessment of treatment response.

Conflict of Interest

The authors declare that they have no conflict of interest.

References

[1] Rajiah P, Parakh A, Kay F et al. Update on Multienergy CT: Physics, Principles, and Applications. Radiographics 2020; 40: 1284–1308. doi:10.1148/rg.2020200038

[2] Agrawal MD, Pinho DF, Kulkarni NM et al. Oncologic applications of dual-energy CT in the abdomen. Radiographics 2014; 34: 589–612. doi:10.1148/rg.343135041

[3] Odisio EG, Truong MT, Duran C et al. Role of Dual-Energy Computed Tomography in Thoracic Oncology. Radiol Clin North Am 2018; 56: 535–548. doi:10.1016/j.rcl.2018.03.011

[4] Meyer M, Hohenberger P, Overhoff D et al. Dual-Energy CT Vital Iodine Tumor Burden for Response Assessment in Patients With Metastatic GIST Undergoing TKI Therapy: Comparison to Standard CT and FDG PET/CT Criteria. Am J Roentgenol 2021. doi:10.2214/Am J Roentgenol.21.26636

[5] Gordic S, Puippe GD, Krauss B et al. Correlation between Dual-Energy and Perfusion CT in Patients with Hepatocellular Carcinoma. Radiology 2016; 280: 78–87. doi:10.1148/radiol.2015151560

[6] Krauss B. Dual-Energy Computed Tomography: Technology and Challenges. Radiol Clin North Am 2018; 56: 497–506. doi:10.1016/j.rcl.2018.03.008

[7] McCollough CH, Leng S, Yu L et al. Dual- and Multi-Energy CT: Principles, Technical Approaches, and Clinical Applications. Radiology 2015; 276: 637–653. doi:10.1148/radiol.2015142631

[8] Almeida IP, Schyns LE, Ollers MC et al. Dual-energy CT quantitative imaging: a comparison study between twin-beam and dual-source CT scanners. Med Phys 2017; 44: 171–179. doi:10.1002/mp.12000

[9] Marin D, Davis D, Roy Choudhury K et al. Characterization of Small Focal Renal Lesions: Diagnostic Accuracy with Single-Phase Contrast-enhanced Dual-Energy CT with Material Attenuation Analysis Compared with Conventional Attenuation Measurements. Radiology 2017; 284: 737–747. doi:10.1148/radiol.2017161872

[10] Botsikas D, Triponez F, Boudabbous S et al. Incidental adrenal lesions detected on enhanced abdominal dual-energy CT: can the diagnostic work-up be shortened by the implementation of virtual unenhanced images? Eur J Radiol 2014; 83: 1746–1751. doi:10.1016/j.ejrad.2014.06.017

[11] Meyer M, Nelson RC, Vernuccio F et al. Virtual Unenhanced Images at Dual-Energy CT: Influence on Renal Lesion Characterization. Radiology 2019; 291: 381–390. doi:10.1148/radiol.2019181100

[12] Van Hedent S, Hokamp NG, Laukamp KR et al. Differentiation of Hemorrhage from Iodine Using Spectral Detector CT: A Phantom Study. AJNR Am J Neuroradiol 2018; 39: 2205–2210. doi:10.3174/ajnr.A5872

[13] Slebocki K, Kraus B, Chang DH et al. Incidental Findings in Abdominal Dual-Energy Computed Tomography: Correlation Between True Noncontrast and Virtual Noncontrast Images Considering Renal and Liver Cysts and Adrenal Masses. J Comput Assist Tomogr 2017; 41: 294–297. doi:10.1097/RCT.0000000000000503

[14] Fabritius G, Brix G, Nekolla E et al. Cumulative radiation exposure from imaging procedures and associated lifetime cancer risk for patients with lymphoma. Sci Rep 2016; 6: 35181. doi:10.1038/srep35181

[15] Kosmala A, Weng AM, Heidemeier A et al. Multiple Myeloma and Dual-Energy CT: Diagnostic Accuracy of Virtual Noncalcium Technique for Detection of Bone Marrow Infiltration of the Spine and Pelvis. Radiology 2018; 286: 205–213. doi:10.1148/radiol.2017170281

[16] Kosmala A, Weng AM, Krauss B et al. Dual-energy CT of the bone marrow in multiple myeloma: diagnostic accuracy for quantitative differentiation of infiltration patterns. Eur Radiol 2018; 28: 5083–5090. doi:10.1007/s00330-018-5537-5

[17] Huang X, Gao S, Ma Y et al. The optimal monoenergetic spectral image level of coronary computed tomography (CT) angiography on a dual-layer spectral detector CT with half-dose contrast media. Quant Imaging Med Surg 2020; 10: 592–603. doi:10.21037/qims.2020.02.17

[18] Grosse Hokamp N, Hoink AJ, Doerner J et al. Assessment of arterially hyper-enhancing liver lesions using virtual monoenergetic images from spectral detector CT: phantom and patient experience. Abdom Radiol (NY) 2018; 43: 2066–2074. doi:10.1007/s00261-017-1411-1

[19] Mohammadinejad P, Baffour FI, Adkins MC et al. Benefits of iterative metal artifact reduction and dual-energy CT towards mitigating artifact in the setting of total shoulder prostheses. Skeletal Radiol 2021; 50: 51–58. doi:10.1007/s00256-020-03528-3

[20] Eichler M, May M, Wiesmueller M et al. Single source split filter dual energy: Image quality and liver lesion detection in abdominal CT. Eur J Radiol 2020; 126: 108913. doi:10.1016/j.ejrad.2020.108913

[21] D'Angelo T, Cicero G, Mazziotti S et al. Dual energy computed tomography virtual monoenergetic imaging: technique and clinical applications. Br J Radiol 2019; 92: 20180546. doi:10.1259/bjr.20180546

[22] Schabel C, Patel B, Harring S et al. Renal Lesion Characterization with Spectral CT: Determining the Optimal Energy for Virtual Monoenergetic Reconstruction. Radiology 2018; 287: 874–883. doi:10.1148/radiol.2018171657

[23] Noda Y, Tochigi T, Parakh A et al. Low keV portal venous phase as a surrogate for pancreatic phase in a pancreatic protocol dual-energy CT: feasibility, image quality, and lesion conspicuity. Eur Radiol 2021; 31: 6898–6908. doi:10.1007/s00330-021-07744-w

[24] Amato C, Klein L, Wehrse E et al. Potenzial of contrast agents based on high-Z elements for contrast-enhanced photon-counting computed tomography. Med Phys 2020; 47: 6179–6190. doi:10.1002/mp.14519

[25] Konstantinides SV, Meyer G, Becattini C et al. 2019 ESC Guidelines for the diagnosis and management of acute pulmonary embolism developed in collaboration with the European Respiratory Society (ERS). Eur Heart J 2020; 41: 543–603. doi:10.1093/eurheartj/ehz405

[26] Gladish GW, Choe DH, Marom EM et al. Incidental pulmonary emboli in oncology patients: prevalence, CT evaluation, and natural history. Radiology 2006; 240: 246–255. doi:10.1148/radiol.2401051129

[27] Uhrig M, Simons D, Schlemmer HP. Incidental pulmonary emboli in stage IV melanoma patients: Prevalence in CT staging examinations and improved detection with vessel reconstructions based on dual energy CT. PLoS One 2018; 13: e0199458. doi:10.1371/journal.pone.0199458

[28] Patel BN, Rosenberg M, Vernuccio F et al. Characterization of Small Incidental Indeterminate Hypoattenuating Hepatic Lesions: Added Value of Single-Phase Contrast-Enhanced Dual-Energy CT Material Attenuation Analysis. Am J Roentgenol 2018; 211: 571–579. doi:10.2214/Am J Roentgenol.17.19170

[29] Herts BR, Silverman SG, Hindman NM et al. Management of the Incidental Renal Mass on CT: A White Paper of the ACR Incidental Findings Committee. J Am Coll Radiol 2018; 15: 264–273. doi:10.1016/j.jacr.2017.04.028

[30] Zarzour JG, Milner D, Valentin R et al. Quantitative iodine content threshold for discrimination of renal cell carcinomas using rapid kV-switching dual-energy CT. Abdom Radiol (NY) 2017; 42: 727–734. doi:10.1007/s00261-016-0967-5

[31] Meyer M, Nelson RC, Vernuccio F et al. Comparison of Iodine Quantification and Conventional Attenuation Measurements for Differentiating Small, Truly Enhancing Renal Masses From High-Attenuation Non-enhancing Renal Lesions With Dual-Energy CT. Am J Roentgenol 2019; 213: W26–W37. doi:10.2214/Am J Roentgenol.18.20547

[32] Jacobsen MC, Schellingerhout D, Wood CA et al. Intermanufacturer Comparison of Dual-Energy CT Iodine Quantification and Monochromatic Attenuation: A Phantom Study. Radiology 2018; 287: 224–234. doi:10.1148/radiol.2017170896

[33] Nagayama Y, Inoue T, Oda S et al. Adrenal Adenomas versus Metastases: Diagnostic Performance of Dual-Energy Spectral CT Virtual Noncontrast Imaging and Iodine Maps. Radiology 2020; 296: 324–332. doi:10.1148/radiol.2020192227

[34] Albrecht MH, Vogl TJ, Martin SS et al. Review of Clinical Applications for Virtual Monoenergetic Dual-Energy CT. Radiology 2019; 293: 260–271. doi:10.1148/radiol.2019182297

[35] Albrecht MH, Scholtz JE, Kraft J et al. Assessment of an Advanced Monoenergetic Reconstruction Technique in Dual-Energy Computed Tomography of Head and Neck Cancer. Eur Radiol 2015; 25: 2493–2501. doi:10.1007/s00330-015-3627-1

[36] Husarik DB, Gordic S, Desbiolles L et al. Advanced virtual monoenergetic computed tomography of hyperattenuating and hypoattenuating liver lesions: ex-vivo and patient experience in various body sizes. Invest Radiol 2015; 50: 695–702. doi:10.1097/RLI.0000000000000171

[37] Kovacs DG, Rechner LA, Appelt AL et al. Metal artefact reduction for accurate tumour delineation in radiotherapy. Radiother Oncol 2018; 126: 479–486. doi:10.1016/j.radonc.2017.09.029

[38] Bar E, Lalonde A, Royle G et al. The potential of dual-energy CT to reduce proton beam range uncertainties. Med Phys 2017; 44: 2332–2344. doi:10.1002/mp.12215

[39] Kornberg A, Schernhammer M, Friess H. (18)F-FDG-PET for Assessing Biological Viability and Prognosis in Liver Transplant Patients with Hepatocellular Carcinoma. J Clin Transl Hepatol 2017; 5: 224–234. doi:10.14218/JCTH.2017.00014

[40] Gupta R, Phan CM, Leidecker C et al. Evaluation of dual-energy CT for differentiating intracerebral hemorrhage from iodinated contrast material staining. Radiology 2010; 257: 205–211. doi:10.1148/radiol.10091806

[41] Apfaltrer P, Meyer M, Meier C et al. Contrast-enhanced dual-energy CT of gastrointestinal stromal tumors: is iodine-related attenuation a potential indicator of tumor response? Invest Radiol 2012; 47: 65–70. doi:10.1097/RLI.0b013e31823003d2

[42] Reimer RP, Hokamp NG, Niehoff J et al. Value of spectral detector computed tomography for the early assessment of technique efficacy after microwave ablation of hepatocellular carcinoma. PLoS One 2021; 16: e0252678. doi:10.1371/journal.pone.0252678

[43] Bolus D, Morgan D, Berland L. Effective use of the Hounsfield unit in the age of variable energy CT. Abdom Radiol (NY) 2017; 42: 766–771. doi:10.1007/s00261-017-1052-4

[44] De Cecco CN, Muscogiuri G, Schoepf UJ et al. Virtual unenhanced imaging of the liver with third-generation dual-source dual-energy CT and advanced modeled iterative reconstruction. Eur J Radiol 2016; 85: 1257–1264. doi:10.1016/j.ejrad.2016.04.012

[45] Faby S, Kuchenbecker S, Sawall S et al. Performance of today's dual energy CT and future multi energy CT in virtual non-contrast imaging and in iodine quantification: A simulation study. Med Phys 2015; 42: 4349–4366. doi:10.1118/1.4922654

[46] Graser A, Johnson TR, Hecht EM et al. Dual-energy CT in patients suspected of having renal masses: can virtual nonenhanced images replace true nonenhanced images? Radiology 2009; 252: 433–440. doi:10.1148/radiol.2522080557

[47] Ho LM, Marin D, Neville AM et al. Characterization of adrenal nodules with dual-energy CT: can virtual unenhanced attenuation values replace true unenhanced attenuation values? Am J Roentgenol 2012; 198: 840–845. doi:10.2214/Am J Roentgenol.11.7316

[48] Lee HA, Lee YH, Yoon KH et al. Comparison of Virtual Unenhanced Images Derived From Dual-Energy CT With True Unenhanced Images in Evaluation of Gallstone Disease. Am J Roentgenol 2016; 206: 74–80. doi:10.2214/Am J Roentgenol.15.14570

[49] Tian SF, Liu AL, Wang HQ et al. Virtual non-contrast computer tomography (CT) with spectral CT as an alternative to conventional unenhanced CT in the assessment of gastric cancer. Asian Pac J Cancer Prev 2015; 16: 2521–2526

[50] Borhani AA, Kulzer M, Iranpour N et al. Comparison of true unenhanced and virtual unenhanced (VUE) attenuation values in abdominopelvic single-source rapid kilovoltage-switching spectral CT. Abdom Radiol (NY) 2017; 42: 710–717. doi:10.1007/s00261-016-0991-5

[51] Olivia Popnoe D, Ng CS, Zhou S et al. Comparison of enhancement quantification from virtual unenhanced images to true unenhanced images in multiphase renal Dual-Energy computed tomography: A phantom study. J Appl Clin Med Phys 2019; 20: 171–179. doi:10.1002/acm2.12685

[52] Popnoe DO, Ng CS, Zhou S et al. Comparison of virtual to true unenhanced abdominal computed tomography images acquired using rapid kV-switching dual energy imaging. PLoS One 2020; 15: e0238582. doi:10.1371/journal.pone.0238582

[53] Kordbacheh H, Baliyan V, Singh P et al. Rapid kVp switching dual-energy CT in the assessment of urolithiasis in patients with large body habitus: preliminary observations on image quality and stone characterization. Abdom Radiol (NY) 2019; 44: 1019–1026. doi:10.1007/s00261-018-1808-5

[54] Xiao JM, Hippe DS, Zecevic M et al. Virtual Unenhanced Dual-Energy CT Images Obtained with a Multimaterial Decomposition Algorithm: Diagnostic Value for Renal Mass and Urinary Stone Evaluation. Radiology 2021; 298: 611–619. doi:10.1148/radiol.2021192448